Materials Characterization 163 (2020) 110248

Contents lists available at ScienceDirect

Materials Characterization

journal homepage: www.elsevier.com/locate/matchar

Impact of Cu^{2+} substitution by Co^{2+} on the structural and magnetic properties of $CuFe_2O_4$ synthesized by sol-gel route

Thomas Dippong[a,*], Iosif Grigore Deac[b], Oana Cadar[c], Erika Andrea Levei[c], Ioan Petean[d]

[a] Technical University of Cluj-Napoca, North University Center of Baia Mare, Department of Chemistry and Biology, 76 Victoriei Street, 430122 Baia Mare, Romania
[b] Babes-Bolyai University, Faculty of Physics, 1 Kogalniceanu Street, 400084 Cluj-Napoca, Romania
[c] INCDO-INOE 2000, Research Institute for Analytical Instrumentation, 67 Donath Street, 400293 Cluj-Napoca, Romania
[d] Babes-Bolyai University, Faculty of Chemistry and Chemical Engineering, 11 Arany Janos Street, 400028 Cluj-Napoca, Romania

ARTICLE INFO

Keywords:
Cu-Co ferrite
Nanocomposites
Sol-gel method
Magnetic properties
Particle size
Roughness

ABSTRACT

The paper presents the influence of Cu^{2+} substitution by Co^{2+} in $CuFe_2O_4$ embedded in SiO_2 on the structure, morphology and magnetic properties. The $CuFe_2O_4/SiO_2$, $Co_{0.25}Cu_{0.75}Fe_2O_4/SiO_2$, $Co_{0.50}Cu_{0.50}Fe_2O_4/SiO_2$, $Co_{0.75}Cu_{0.25}Fe_2O_4/SiO_2$ and $CoFe_2O_4/SiO_2$ nanocomposites (NCs) were obtained by sol-gel method followed by annealing at 500, 800 and 1100 °C. Beside the ferrite, the presence of CuO at low temperature and cristobalite and quartz at high temperature were observed. The size of spherical particles increases from 38 to 85 nm with increasing annealing temperature and Co^{2+} content. The saturation magnetization, remanent magnetization, coercive field and magnetic anisotropy increase by substituting Cu^{2+} with Co^{2+} in the $CuFe_2O_4$ structure. The NCs have superparamagnetic and ferromagnetic behavior.

1. Introduction

A high number of researches focused on magnetic nanomaterials development, characterization and application in various fields [1–13]. Ferrites with tunable magnetic, optical and electrical properties are of great interest for a broad range of technological applications. Their properties are influenced by the synthesis route, chemical composition, thermal treatment (duration and temperature) and the cation distribution among tetrahedral (A) and octahedral (B) sites [4–6]. $CoFe_2O_4$ is a ferromagnetic ceramic with multiple properties, such as high anisotropy constant (K), coercivity (H_C) and Curie temperature, moderate saturation magnetization (M_S), excellent chemical and mechanical stability, large magnetostrictive coefficient (λ), high electrical resistance and low eddy current losses [1,2,4–6].

In the last years, numerous efforts have been focused on processing and chemical modifications of $CoFe_2O_4$ to obtain enhanced magnetic and magnetostrictive properties. In this regard, the annealing of $CoFe_2O_4$ results in the modification of cation distribution between the octahedral and tetrahedral sites and the improvement of magnetic properties [3,4]. Regarding the compositional alterations, it was observed that the substitution of Co^{2+} with Cu^{2+} in Co−Cu ferrite results in moderate values of λ and M_S and substantial decreases in H_C and Curie temperature [3].

The $CoFe_2O_4$ crystallizes in a cubic spinel structure with the Co^{2+} ions in octahedral sites and Fe^{3+} ions equally-distributed between tetrahedral and octahedral sites [2,3,14,15]. The crystal lattice of $CuFe_2O_4$ exhibits a tetragonal distortion of the inverse spinel with Cu^{2+} ions fully occupying the octahedral sites, whereas Fe^{3+} ions occupying both octahedral and tetrahedral sites [16,17]. As the magnetic moment and the ionic radius of Cu^{2+} ions is different from that of Co^{2+} ions, the substitution of Cu^{2+} with Co^{2+} in Cu−Co ferrite results in distorted spinel structures depending on the Cu/Co molar ratio and the applied thermal treatment leading to the modification of the structural, vibrational, dielectric and magnetic properties, also correlated with the particle size and the synthesis conditions [1–3,14,15,18,19]. In order to obtain the desired magnetic properties, such as good H_C and M_S, it is very important to use an appropriate ratio between Co^{2+} and Cu^{2+} ions [17–19]. The annealing temperature also influences the permeability at low frequencies and low values of alternating magnetic field and the parameters of ferromagnetic resonance [7,8,15–19].

Tetraethyl orthosilicate (TEOS) is a commonly-used network forming agent in the sol-gel synthesis, as it forms robust networks with moderate reactivity, have short gelation time and allows the incorporation of a broad range of organic and inorganic molecules. Moreover, by variation of the synthesis conditions (pH, temperature) allows the control of nucleation and growth [20–22].

Cu−Co ferrite is a promising functional material for various fields such as electronics, optoelectronics, magnetoelectronics,

* Corresponding author.
E-mail address: dippong.thomas@yahoo.ro (T. Dippong).

https://doi.org/10.1016/j.matchar.2020.110248
Received 17 January 2020; Received in revised form 26 February 2020; Accepted 4 March 2020
Available online 05 March 2020

electrochemistry, photocatalysis, medicine and biotechnology because of its low cost, environmental benignity, biocompatibility, chemical stability, interesting magnetic behavior and high resistance to corrosion [1–3,9–15,18,19]. Most of the applications depend on the magnetic properties of these materials determined by the complex interplay of several factors among which distribution and spin canting are the most important [15].

The aim of this study is the synthesis and characterization of Cu−Co ferrites embedded in SiO_2 matrix obtained by sol-gel synthesis and post-annealing pathway. The crystalline phases were identified by X-ray diffraction (XRD), the formation of ferrite and SiO_2 matrix was monitored by Fourier transform infrared spectroscopy (FT-IR), the shape, agglomeration, surface roughness and particle size by atomic force microscopy (AFM), while the magnetic properties were investigated by vibrating sample magnetometer (VSM). The change in the structural and magnetic properties with the substitution of Cu^{2+} with Co^{2+} in the Cu ferrite structure, and the influence of crystalline phases and particle size on the magnetic properties were also assessed.

2. Experimental

Nanocomposites (NCs) of Cu−Co ferrite embedded in SiO_2 matrix (45% wt. ferrite, 55% wt. SiO_2) were synthesized by sol-gel method using $Cu(NO_3)_2{\cdot}3H_2O$, $Co(NO_3)_2{\cdot}6H_2O$, $Fe(NO_3)_3{\cdot}9H_2O$, 1,4-butanediol (BD), tetraethyl orthosilicate (TEOS, 98%), ethanol and HNO_3 65%, using Cu:Co:Fe molar ratio of 1:0:2, 3:1:8, 1:1:4, 1:3:8, 0:1:2 and nitrate:BD:TEOS molar ratio of 1:1:1.22. After gelation at room temperature, the samples were grinded and thermally treated at 500 °C for 5 h, then at 800 °C and 1100 °C for 5 h.

The obtained $CuFe_2O_4$, $Co_{0.25}Cu_{0.75}Fe_2O_4$, $Co_{0.50}Cu_{0.50}Fe_2O_4$, $Co_{0.75}Cu_{0.25}Fe_2O_4$ and $CoFe_2O_4/SiO_2$ NCs were characterized by XRD, FT-IR, AFM and VSM. The FT-IR spectra were recorded on 1% KBr pellets using a Spectrum BX II (Perkin Elmer) spectrometer. The XRD patterns were recorded using a D8 Advance (Bruker) diffractometer with $CuK_{\alpha 1}$ radiation (λ = 1.54056 Å). AFM was performed with a JSPM 4210 (JEOL) scanning probe microscope using NSC15 cantilevers (diamond coated silicon nitride tips) having a resonant frequency of 325 kHz and a force constant of 40 N/m in tapping mode. The samples were dispersed into ultrapure water and transferred on glass slides by vertical adsorption for 30 s, followed by natural drying. The dried slides were scanned at different sizes over areas of approximately 2.5 μm × 2.5 μm to 1 μm × 1 μm, for three different macroscopic sites. The best results were obtained at 1 μm × 1 μm proving that obtained NCs adsorbed on the solid substrate are nano-structured. The obtained AFM images were processed and analyzed using Win SPM 2.0 Processing software. The content of Cu, Co and Fe in the NCs annealed at 1100 °C was determined by a handheld energy dispersive X-ray fluorescence spectrometer (XRF, Innov-X Alpha 6500) with X-ray tube, W anode and Si PiN diode detector. SEM images were recorded using a Hitachi SU8230 microscope, while TEM images were recorded using a Hitachi HD2700 electron microscope coupled with an X-Max 1160 EDX detector (Oxford Instruments). A vibrating sample cryogen-free VSM magnetometer (Cryogenic Limited) was used for magnetic measurements. The hysteresis loops were recorded in magnetic fields from −2 to 2 T, at room temperature. Magnetization *vs.* magnetic field measurements were performed to find M_S up to 5 T.

3. Results and discussion

The XRD patterns of NCs at 500, 800 and 1100 °C are presented in Fig. 1. The identification of phases was carried out by comparing the obtained data with standard diffraction patterns. The XRD patterns of NCs annealed at 500 °C exhibit less intense, broadened peaks, while those annealed at 1100 °C produce more intense and sharp peaks, indicating that the crystallinity of the NCs improves with increasing annealing temperature. A possible explanation could be that at high annealing temperatures, the lattice defects and strains decrease, while the coalescence processes intensify, favoring the increase of grain size [23–26]. At 500 and 800 °C, the low crystalline $CuFe_2O_4$ spinel (JCPDS card no. 73-2315 [27]) fits to *Fd3m* space group as main phase, and CuO (JCPDS card no. 89-5895 [27]) with a monoclinic structure fits to *C2/c* space group as secondary phase. At 1100 °C, SiO_2 (cristobalite) main crystalline phase in agreement with JCPDS card no. 89-3434 [27], and much better crystalized $CuFe_2O_4$ secondary phase are remarked. The XRD patterns of mixed Co−Cu ferrite based NCs reveals that by increasing the Cu^{2+} content, the ferrite diffraction peaks intensify, leading to higher degree of crystallization. At 500 and 800 °C, the diffraction peaks of CuO decrease and the diffraction halo of the amorphous SiO_2 is clearly highlighted at 20-30°, while at 1100 °C, beside Co−Cu ferrite and SiO_2 (cristobalite) crystalline phases, SiO_2 (quartz) crystalline phase (JCPDS card no. 78-1254) also appears [27].

The presence of two crystalline phases (ferrite and SiO_2 as quartz or cristobalite) and the lack of peak shifts in the XRD pattern confirm the formation of NC. Single phase Co ferrite (JCPDS card no. 02-1045 [27]) is obtained at all annealing temperatures, the highest crystallinity being observed after annealing at 1100 °C. No other impurity peak was detected. The presence of crystalline phases resulted from the interaction of metal ions with the SiO_2 matrix was not observed.

The average crystallite size of ferrites estimated by Scherrer equation using the most intense diffraction peak are presented in Table 1 [1,23,26]. The crystallite size (Table 1) decreases from 43.2 to 27.4 nm (500 °C), from 63.7 to 33.1 nm (800 °C) and from 83.4 nm to 38.2 nm (1100 °C), concomitantly with decreasing Cu^{2+} and increasing Co^{2+} content. A possible explanation could be that Cu^{2+} obstructs the particle growth of the spinel structure. Another explanation could be the weak diffraction peaks of $CuFe_2O_4$ in tetragonal crystal structure that appears due to the Jahn-Teller effect in case of high Cu^{2+} contents [1].

The FT-IR spectra of NCs at 500, 800 and 1100 °C are presented in Fig. 2. The FT-IR spectrum of $CuFe_2O_4$ spinel confirms the XRD results by the presence of bands at 578–622 cm^{-1} attributed to the stretching vibration of the Cu−O bonds from tetrahedral sites and the bands at 457–495 cm^{-1}, attributed to the stretching vibration of Fe−O bonds from octahedral sites [1,28–31]. The shift of bands from 578 to 594 cm^{-1} (at 500 and 800 °C) and to 622 cm^{-1} (at 1100 °C) could be explained by the existence of two compounds containing Cu−O bonds ($CuFe_2O_4$ and CuO) at low temperatures, and only $CuFe_2O_4$ at 1100 °C. In all spectra, the characteristic bands of SiO_2 matrix were identified: the bands at 1073–1094 cm^{-1} attributed to the stretching and bending vibration of the Si-O-Si bonds, at 1587–1654 cm^{-1} ascribed to the deformation vibration of the H-OH bonds. The band at 1198 cm^{-1} present only in NCs annealed at 1100 °C is attributed to the Si−O bonds in the SiO_2 (cristobalite) structure [25,27,31].

The FT-IR bands of mixed Co−Cu ferrites are similar to those of $CuFe_2O_4$. However, in the case of NCs with high Co^{2+} content ($Co_{0.75}Cu_{0.25}Fe_2O_4$, $Co_{0.75}Cu_{0.25}Fe_2O_4$), some supplementary bands appears at 599–602 cm^{-1} attributed to the vibration of Co−O bond when the Co^{2+} occupies the octahedral sites and at 459–479 cm^{-1} attributed to the vibration of Fe−O bonds when the Fe^{3+} occupy the tetrahedral sites [2].

The supplementary band at 412–413 cm^{-1} is attributed to the Si−O bond vibration in crystalline quartz (SiO_2) identified by the XRD as second crystalline phase beside cristobalite. The FT-IR spectra show the Co−O and Fe−O vibration bands at 586–601 cm^{-1} and 461–472 cm^{-1} that confirms the presence of Co ferrite. The shift to higher wavenumbers of these two bands could be explained by the higher crystallinity of ferrite at 1100 °C. The bands attributed to Cu−O vibration (620 cm^{-1}) and Si−O (1200 cm^{-1}) vibration belonging to cristobalite disappear.

The NCs annealed at 500, 800 and 1100 °C have an agglomerated aspect mainly related to the coalescence between the finest particles, making difficult their morphological observation. The AFM images of the thin film formed from aqueous dispersions show that all NCs are

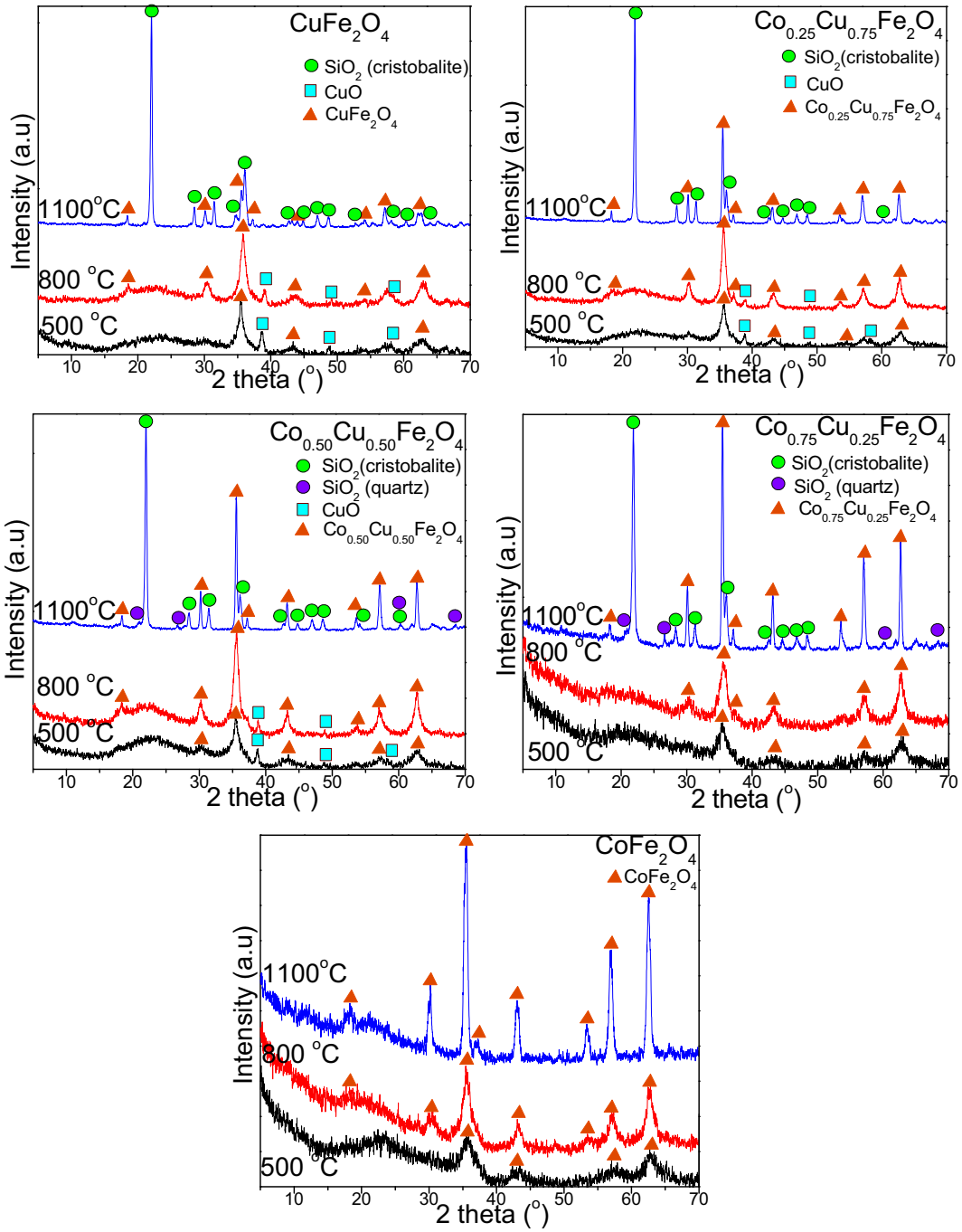

Fig. 1. XRD patterns of $CuFe_2O_4/SiO_2$, $Co_{0.25}Cu_{0.75}Fe_2O_4/SiO_2$, $Co_{0.50}Cu_{0.50}Fe_2O_4/SiO_2$, $Co_{0.75}Cu_{0.25}Fe_2O_4/SiO_2$, $CoFe_2O_4/SiO_2$ NCs annealed at 500, 800 and 1100 °C.

nanostructured (Fig. 3). It means that the ferrite powders dispersed into the water leads to the individualization of particles. The nanoparticles shape and size observed by AFM are in good agreement with literature data [25,29]. Some previous AFM studies on Co ferrite nanoparticles obtained *via* precipitation from solution have ultra-small size and spherical shape [30].

Based on the topographic images (Figs. 3 and 4), data on particle shape and size, morphology of the adsorbed film, surface height and roughness were obtained (Table 1). The morphology of ferrite nanoparticles thin film assembled by adsorption from aqueous dispersion depends mainly on their size, but their density on the surface as well as cluster formation tendency could also affect the surface height and roughness. In case of NCs annealed at 500 °C, the smaller ferrite nanoparticles form dense and uniform films which lead to low roughness values. In case of NCs annealed at 1100 °C, the larger ferrite nanoparticles exhibit an individualization trend which often forms rarefied films with increasing roughness.

Cu ferrite (Fig. 3a-c) presents spherical shape nanoparticles, with size depending on the annealing temperature. The average particles size increases from 45 to 85 nm with increasing annealing temperature and affects the thin film morphology by increasing the surface roughness. At low temperature, a uniform deposit of nanoparticles with low roughness (1 nm) is observed. At high temperature, the film roughness increases about 15 times due to nanoparticle's size and well individualization. AFM observations reveal that Cu ferrite forms the biggest nano-particles. Their three-dimensional aspect is better

Table 1
Sample parameters measured with AFM, XRD and VSM.

Sample	Temperature (°C)	Height (nm)	Roughness (nm)	AFM particle size (nm)	XRD crystallite size (nm)	Anisotropy constant K·10^3 (erg/cm^3)
$CuFe_2O_4$	500	11.0	1.23	45	43.2	0.003
	800	4.6	0.62	65	63.7	0.047
	1100	78.0	15.1	85	83.4	0.178
$Co_{0.25}Cu_{0.75}Fe_2O_4$	500	8.0	1.05	40	37.4	0.113
	800	12.0	1.85	56	55.6	0.074
	1100	4.7	0.59	70	66.8	0.271
$Co_{0.50}Cu_{0.50}Fe_2O_4$	500	4.5	0.59	35	33.8	0.020
	800	10.0	1.56	50	48.1	0.113
	1100	13.0	2.31	60	58.6	0.388
$Co_{0.75}Cu_{0.25}Fe_2O_4$	500	7.0	0.89	30	28.3	0.041
	800	7.0	0.81	45	43.4	0.163
	1100	7.0	1.12	53	52.1	0.826
$CoFe_2O_4$	500	9.0	1.13	30	27.4	0.070
	800	4.7	0.56	35	33.1	0.389
	1100	6.0	0.90	40	38.2	2.219

observed in Fig. 4. The finest nanoparticles are formed by Co ferrite (Fig. 3m-o). These are very small spherical nanoparticles which forms uniform and dense films with low roughness. The particle size is also depending on the annealing treatment, being about 30 nm at low temperatures and 40 nm at high temperatures. At low annealing temperature, the nanoparticles tend to form a very dense film and show a coalescence tendency in partial areas with bi and tri layer adsorbed. This tendency leads to a slightly increased roughness compared to the films resulted at higher temperatures (Table 1).

The adsorbed films at 800 and 1100 °C is uniform but not so dense, the surface roughness is < 1 nm and nano-particles are well-individualized. The mixed ferrites present an intermediary nanostructure between Cu ferrite and Co ferrite (Fig. 3d-l). The surface topography reveals well-individualized spherical nanoparticles. The Co^{2+} addition to Cu ferrite leads to a significant reduction of nanoparticle size, the average size of the mixed ferrites being lower than those of Cu ferrite and higher than those of Co ferrite.

The nanoparticle size determined by AFM is in accordance with the crystallite size estimated by XRD (Table 1), confirming the good dispersion of the nanoparticles in aqueous environment and formation of uniform thin film on the solid substrate. The film roughness depends mainly of nanoparticle size and their surface density. The three-dimensional topographic images (Fig. 3) reveals the dependence of surface roughness on the nanoparticle size, showing the decreasing of nanoparticle size with increasing Co^{2+} content. The Co^{2+} content and annealing temperature are the most important process parameters which influences the nanoparticle size and surface roughness. As the Co^{2+} content determines the magnetic properties of the ferrite compounds as well as nanoparticle size, it could be a start for tailored design of Co−Cu ferrite thin films with a controlled nanoparticle size, surface roughness and magnetic properties.

The XRF data are in good agreement with the theoretical stoichiometric calculations. The SEM images and the elemental distribution maps (Cu, Co, Fe, O, Si) based on TEM-EDX data for NCs annealed at 1100 °C are presented in Fig. 5. The SEM images reveal small irregular shape agglomerations with relatively narrow particle size distribution (40–90 nm). The surface morphology shows a coalescing behavior of the agglomerated particles, which could be due to interfacial surface tension phenomena [26,31]. According to the elemental distribution maps, the elements are uniformly distributed in the sample and the resulted structure is a NC composed of Co−Cu ferrite embedded in SiO_2 matrix. The weight %, atomic % and atomic ratio of Cu−Co ferrites were confirmed TEM-EDX (Table 2). The obtained data are in accordance with the theoretical stoichiometric composition.

The dependence of the magnetization (*M-H* curve) and derivative of magnetization ($dM/d(\mu_oH)$) on the magnetic field for $CuFe_2O_4$, $Co_{0.25}Cu_{0.75}Fe_2O_4$, $Co_{0.50}Cu_{0.50}Fe_2O_4$, $Co_{0.75}Cu_{0.25}Fe_2O_4$ and $CoFe_2O_4$ embedded in SiO_2 matrix are depicted in Figs. 6 and 7. The saturation magnetization (M_S), coercivity (H_C) and remanent magnetization (M_R) were extracted from the magnetic hysteresis loops [25,32].

At all annealing temperatures, the hysteresis loops reveal an increase of the M_S and H_C with increasing Co^{2+} content in the NCs, as a consequence of the replacement of a low magnetic moment ion (1 μ_B), such as Cu^{2+}([Ar]3d^9) with Co^{2+}([Ar]3d^7), having a higher magnetic moment (3μ_B). The Cu^{2+} positioned in the octahedral B-sites of the unit cell has small magnetic moments. When Co^{2+} with higher magnetic moment replaces Cu^{2+}, a decrease of the ferromagnetic (anti-parallel) coupling between tetrahedral (A) and octahedral (B) sites appears, resulting in enhanced M_S [19,23]. In this way, the increase of Co^{2+} content in Cu ferrite depreciates the A-site magnetization and improves the global magnetization [1]. The ferromagnetism in ferrites results, mainly, from A-B super-exchange interaction [1,19]. The ideal unit cell of a pure inverse spinel ferrite has all the Co^{2+} placed in octahedral (B) sites.

The global magnetization is given by the ferromagnetic coupling of the magnetic moments from A and B sites. When Cu^{2+} partially replaces the Co^{2+} in the ferrite structure, a decrease of the M_S will result. The magnetic moment of Fe^{3+} is 5 μ_B for both A and B sites, while that of Co^{2+} and Cu^{2+} ions are 3 μ_B and 1 μ_B, respectively [3,25]. The Co−Cu ferrite is a mixed ferrite. Co ferrite is a hard-magnetic material having high H_C and moderate M_S, while Cu ferrite is a soft magnetic material [30,32]. The K is related to the energy required to change the orientation of the magnetic moment in a magnetic material [24]. The values of K in ferrite are significantly smaller for Cu^{2+} than those for Co^{2+}, resulting in a decrease of the magnetocrystalline K for high Cu^{2+} content [3]. The K increases when magnetic ions (Co^{2+}) are placed in the sites of a mixed spinel structure (Table 1) [26].

The M_S, M_R and H_C increase with increasing annealing temperature as a consequence of the changes determined by high annealing temperature in the shape of the nanoparticles, the surface spin disorder, the pinning of the magnetic moment, the canting of spins, the defects and the particle sizes distribution [3,19]. A spin disorder occurs on the surfaces of the nanoparticles due to the broken chemical bonds and to the high values of the magnetic anisotropy. The high surface to volume ratio makes the surface effects very significant resulting in a lower magnetization of the ferrite nanoparticles in comparison with that of the micron-size ferrites or bulk ferrites. The higher is the annealing temperature, the larger are the particle sizes. The spin and chemical disorder as well as the surface to volume ratio reduces at the surface of the particles.

The K and H_C increase, and this can be related with the critical particle size, magnetic domains structure (M_R) and magneto-crystalline anisotropy [1]. The NCs are mostly, single magnetic domain particles with high magneto-crystalline anisotropy and are in the blocked state at

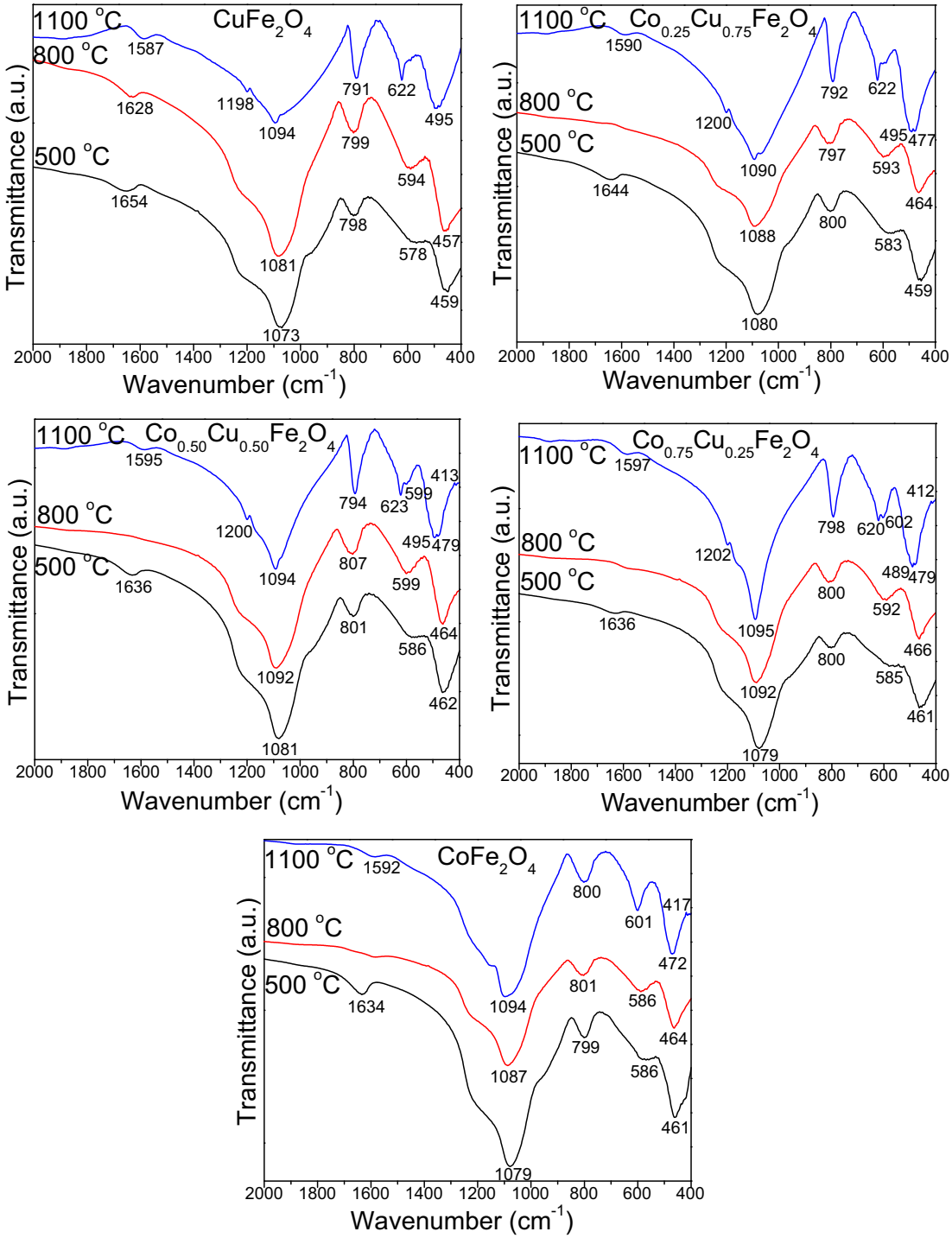

Fig. 2. FT-IR spectra of $CuFe_2O_4/SiO_2$, $Co_{0.25}Cu_{0.75}Fe_2O_4/SiO_2$, $Co_{0.50}Cu_{0.50}Fe_2O_4/SiO_2$, $Co_{0.75}Cu_{0.25}Fe_2O_4/SiO_2$, $CoFe_2O_4/SiO_2$ NCs annealed at 500, 800 and 1100 °C.

300 °C [19]. The shape of the hysteresis loops and the low values of M_S for the NCs annealed at low temperatures indicate a super-paramagnetic-like behavior. The NCs annealed at high temperatures show a ferromagnetic behavior that enhances with increasing of the substitution degree of the Cu^{2+} with Co^{2+}. As expected, the "most" ferromagnetic sample is $CoFe_2O_4$ annealed at 1100 °C [19].

As results from the XRD and AFM data, the crystalline cristobalite phase induced by the presence of SiO_2 matrix improves the structural and morphological properties of NCs. However, the presence of cristobalite depreciates the magnetic properties, due to its diamagnetic character. When the ferrite particles are embedded in the SiO_2 matrix, the enhanced disorder induced at the surface of the ferrite particles will depreciate the magnetic properties, as proven in a previously research [33].

The curves of magnetization derivative ($dM/d(\mu 0H)$) *vs.* applied magnetic field (Fig. 7) display a single peak suggesting pure magnetic phases in our NCs. The larger is the widths of these peaks, the broader is the particle size distribution. The magnetic properties and the topological configuration of these nanoparticles embedded in SiO_2 matrix can be tuned by the annealing temperatures and by the cations ratio to meet

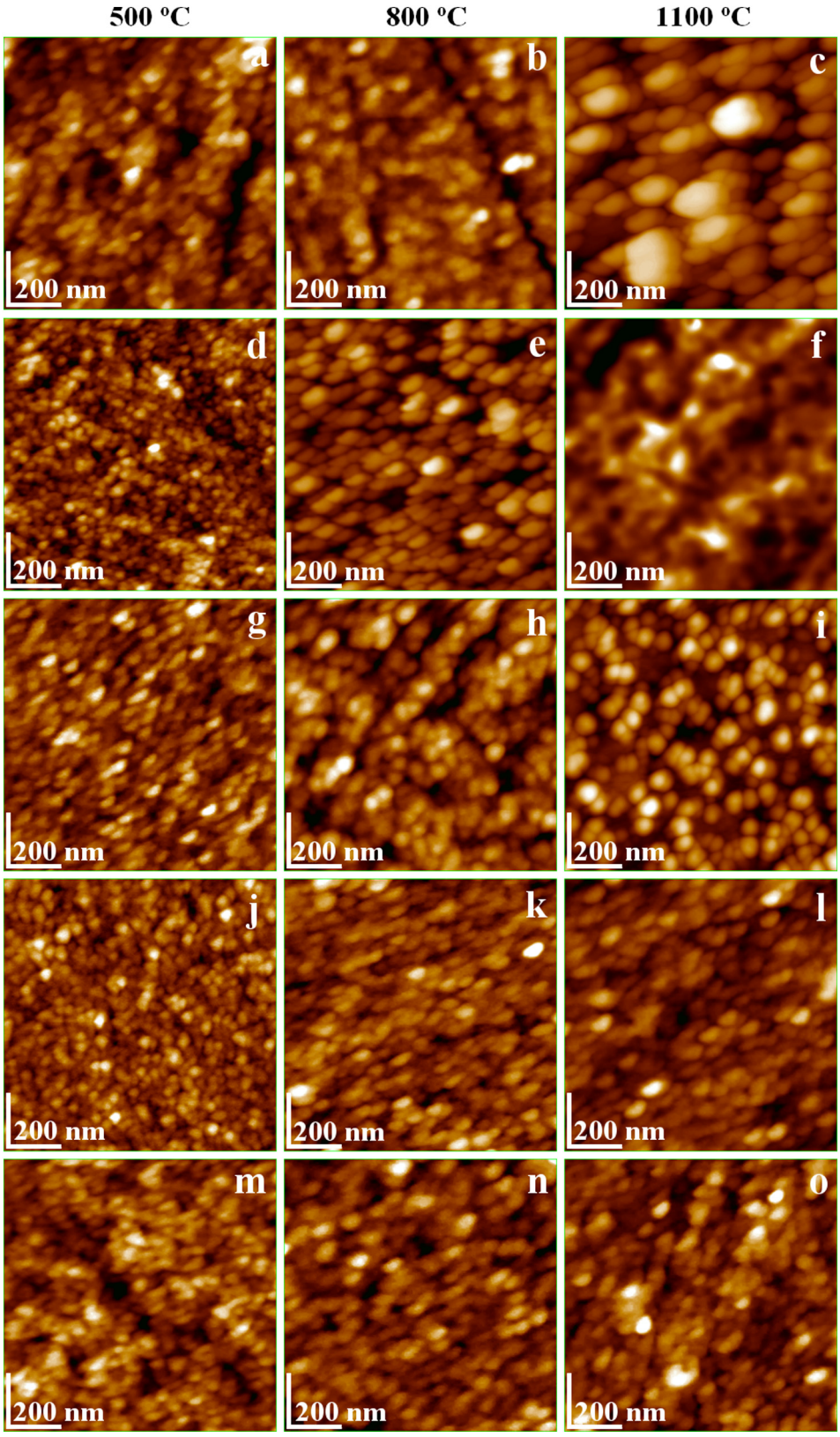

Fig. 3. Topographical AFM images of $CuFe_2O_4$ (a, b, c), $Co_{0.25}Cu_{0.75}Fe_2O_4$ (d, e, f), $Co_{0.50}Cu_{0.50}Fe_2O_4$ (g, h, i), $Co_{0.75}Cu_{0.25}Fe_2O_4$ (j, k, l) and $CoFe_2O_4$ (m, n, o) NCs annealed at 500, 800 and 1100 °C.

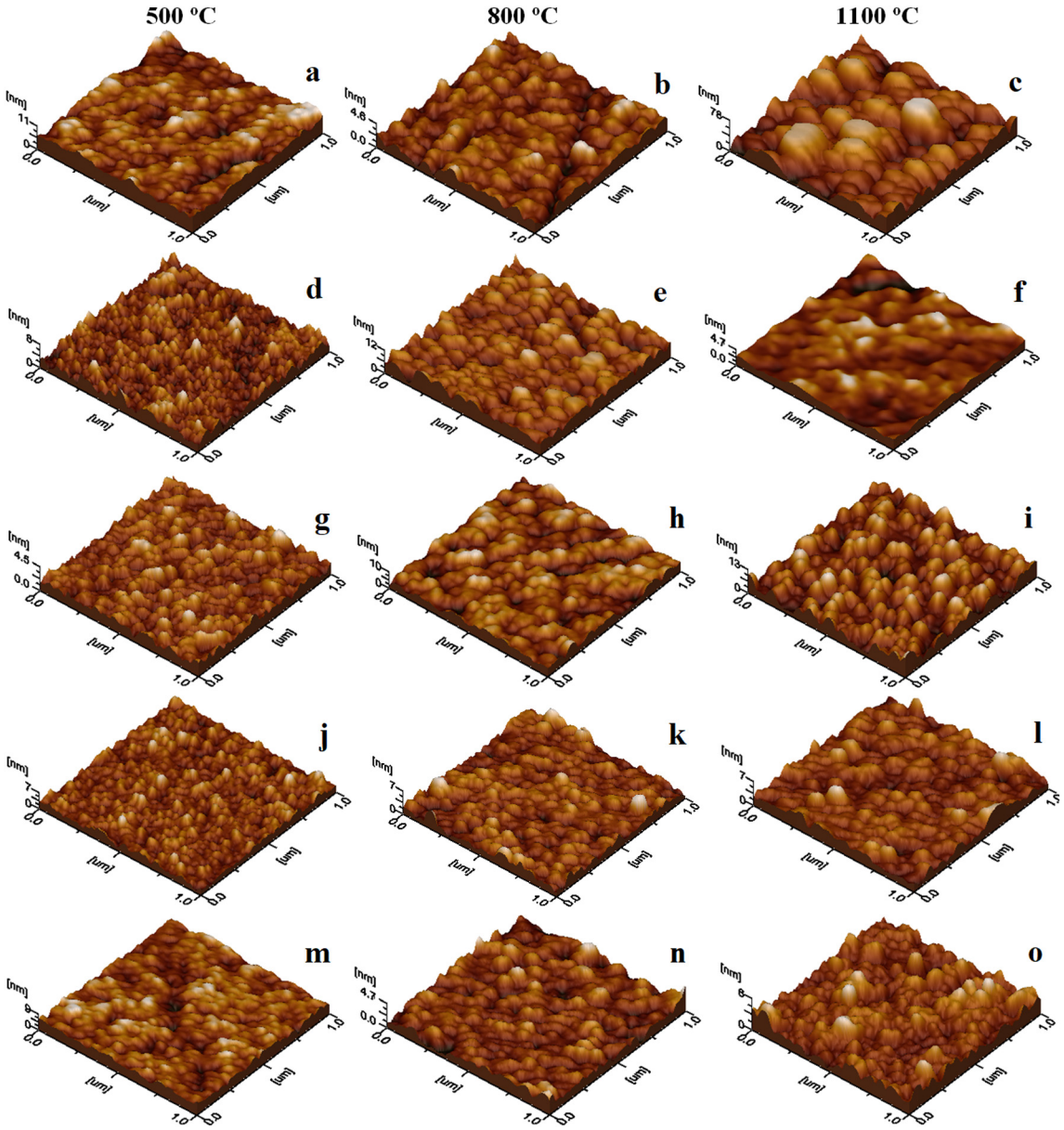

Fig. 4. AFM three-dimensional topographic images of $CuFe_2O_4$ (a, b, c), $Co_{0.25}Cu_{0.75}Fe_2O_4$ (d, e, f), $Co_{0.50}Cu_{0.50}Fe_2O_4$ (g, h, i), $Co_{0.75}Cu_{0.25}Fe_2O_4$ (j, k, l) and $CoFe_2O_4$ (m, n, o) NCs annealed at 500, 800 and 1100 °C.

the specifications for various technical applications.

4. Conclusions

The XRD and AFM investigations showed that the ferrite powders synthesized in this paper are nanocrystalline and produce uniform films by dispersion in aqueous environment. According to XRD and FT-IR investigations, at 500 and 800 °C, $CuFe_2O_4$ is impurified by CuO, while at 1100 °C by SiO_2 (cristobalite) crystalline phases. By increasing the Co^{2+} content, the degree of crystallization of Cu−Co ferrite increases, while the content of CuO (at 500 and 800 °C) and SiO_2 (cristobalite) decreases and SiO_2 (quartz) increases (at 1100 °C). In all cases, the ferrite was the single magnetic crystalline phase. Among the investigated NCs, Cu ferrite forms the biggest and Co-ferrite the smallest particles. The Co^{2+} addition to Cu-ferrite leads to significant size decrease and improve the uniformity of adsorbed layers. The magnetic parameters, namely M_S (1.2–30.2 emu/g), M_R (0.01–15.1 emu/g), H_C (0.004–0.117 T) and K ($0.003{\cdot}10^{-3}$-$2.219\ 10^{-3}$ erg/cm^3) enhance, while crystallite size decreas by substituting Cu^{2+} with Co^{2+} in the ferrite structure. Besides, the magnetic parameters, the crystallite and particle sizes increase by increasing the annealing temperature. The magnetic measurements revealed that AB super-exchange interaction is depreciated when Co^{2+} partially replace Cu^{2+} in $CuFe_2O_4$, improving the H_C and M_S. The NCs annealed at low temperatures exhibit a superparamagnetic behavior, while the NCs annealed at high temperatures have a ferromagnetic behavior. The synthesized NCs are potential candidates to be used in thin-film technology. The physical properties of such films can be tuned by controlling Co^{2+} content and the annealing temperature.

Declaration of competing interest

The authors declare that they have no known competing financial interests or personal relationships that could have appeared to influence the work reported in this paper.

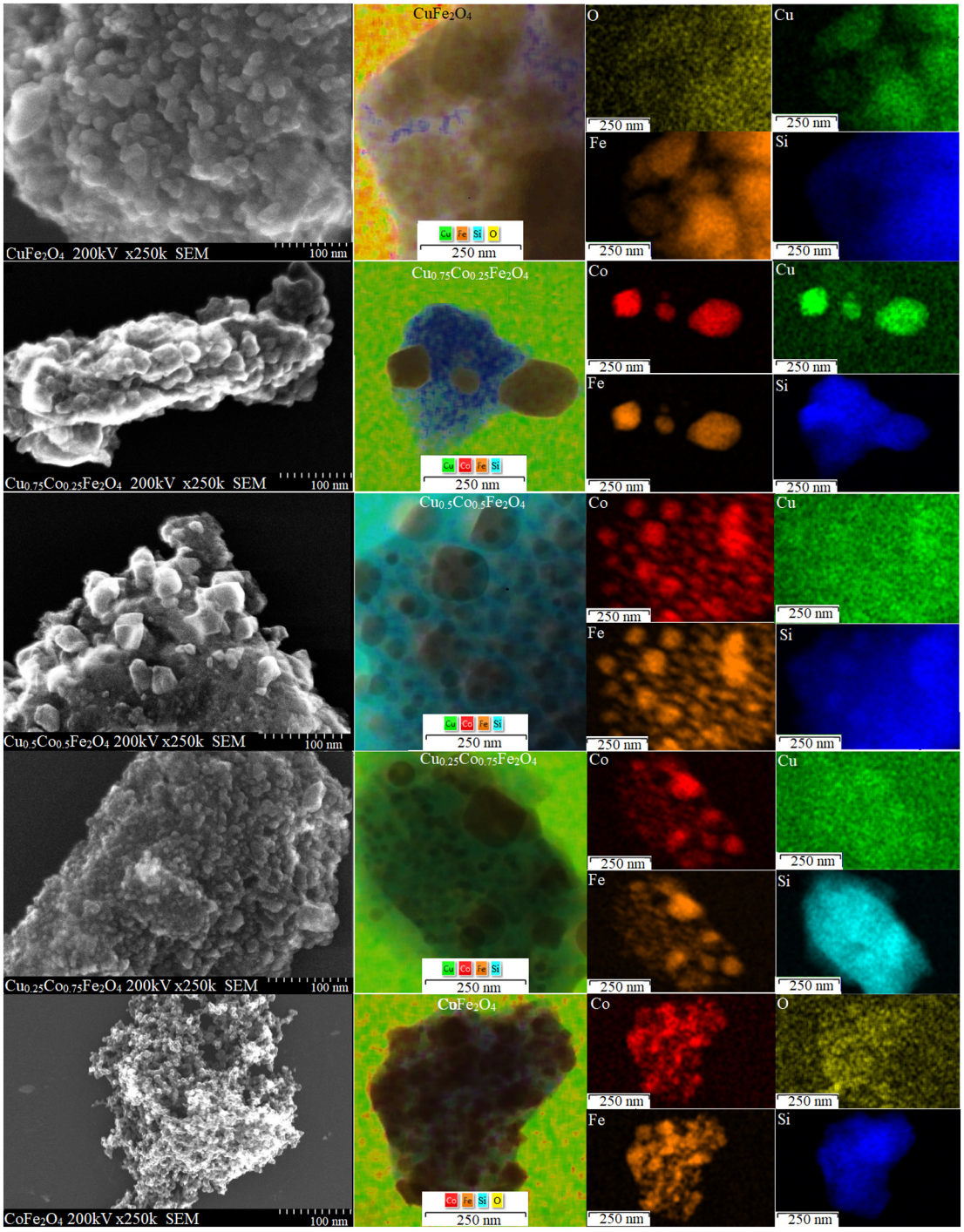

Fig. 5. SEM images and element distribution maps of $CuFe_2O_4/SiO_2$, $Co_{0.25}Cu_{0.75}Fe_2O_4/SiO_2$, $Co_{0.50}Cu_{0.50}Fe_2O_4/SiO_2$, $Co_{0.75}Cu_{0.25}Fe_2O_4/SiO_2$, $CoFe_2O_4/SiO_2$ NCs annealed at 1100 ˚C.

Table 2
The weight %, atomic % and atomic ratio of elements (Cu:Co:Fe:O) in Co–Cu ferrite annealed at 1100 ˚C revealed by TEM-EDX data.

Molecular formula (theoretical)	Weight %				Atomic %				Atomic ratio				Redefined molecular formula
	Cu	Co	Fe	O	Cu	Co	Fe	O	Cu	Co	Fe	O	
$CuFe_2O_4$	27.1	0.0	45.8	27.1	14.5	0	28.0	57.5	1.02	0	1.96	4.04	$Cu_{1.02}Fe_{1.96}O_{4.04}$
$Co_{0.25}Cu_{0.75}Fe_2O_4$	6.2	19.3	47.1	27.4	3.3	11.0	28.3	57.4	0.23	0.77	1.98	4.02	$Co_{0.23}Cu_{0.77}Fe_{1.98}O_4$
$Co_{0.50}Cu_{0.50}Fe_2O_4$	13.7	12.4	46.9	27.0	7.3	7.2	28.5	57.0	0.51	0.50	1.99	3.99	$Co_{0.51}Cu_{0.50}Fe_{1.99}O_{3.99}$
$Co_{0.75}Cu_{0.25}Fe_2O_4$	19.8	6.4	47.0	26.9	10.6	3.7	28.6	57.1	0.74	0.26	2.01	4.01	$Co_{0.74}Cu_{0.26}Fe_{2.01}O_{4.01}$
$CoFe_2O_4$	0.0	24.8	48.2	27.0	0	14.2	29.0	56.8	0	0.99	2.03	3.97	$Co_{0.99}Fe_{2.03}O_{3.97}$

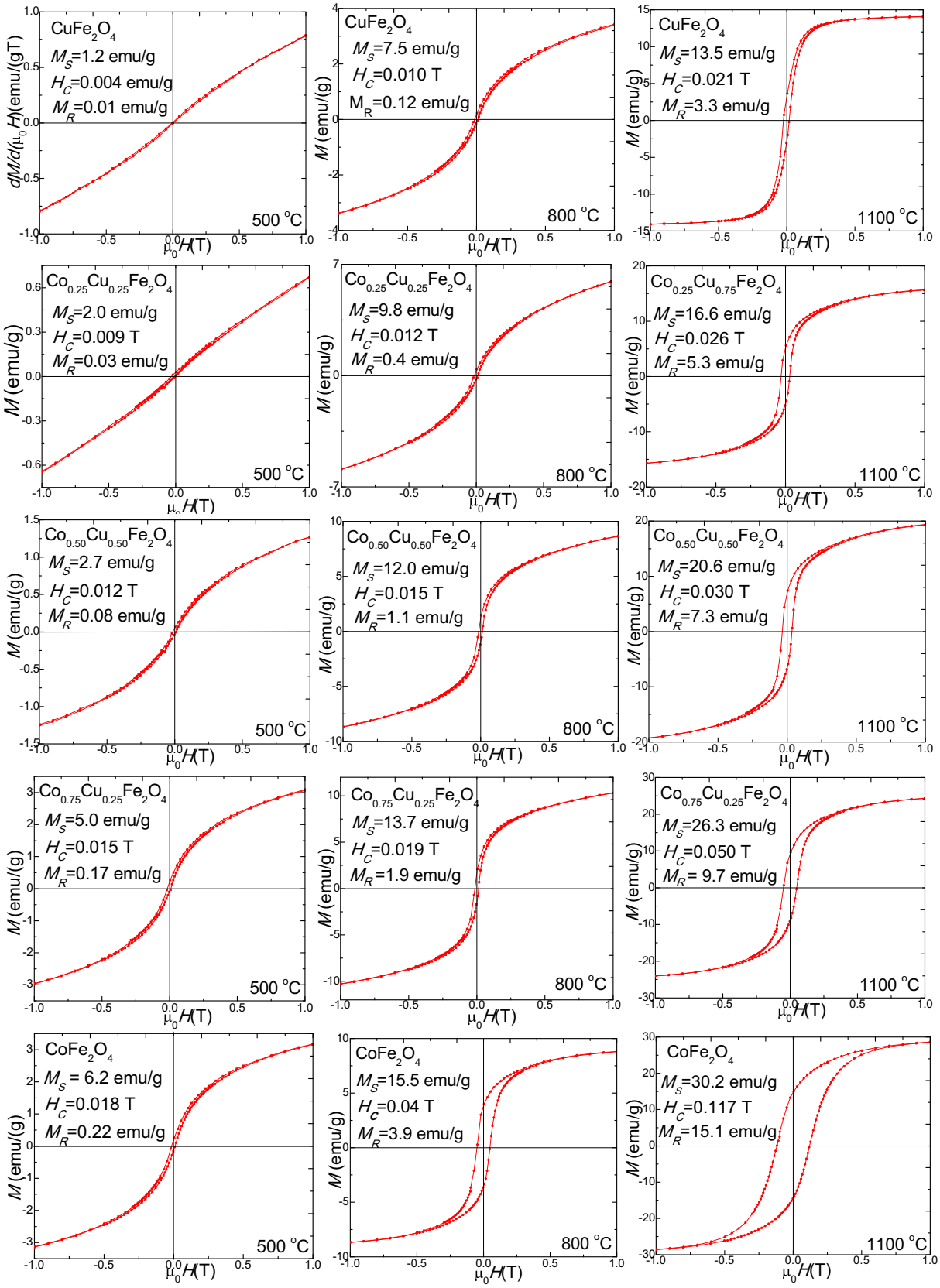

Fig. 6. Magnetic hysteresis loops of $CuFe_2O_4/SiO_2$, $Co_{0.25}Cu_{0.75}Fe_2O_4/SiO_2$, $Co_{0.50}Cu_{0.50}Fe_2O_4/SiO_2$, $Co_{0.75}Cu_{0.25}Fe_2O_4/SiO_2$, $CoFe_2O_4/SiO_2$ annealed at 500, 800 and 1100 °C.

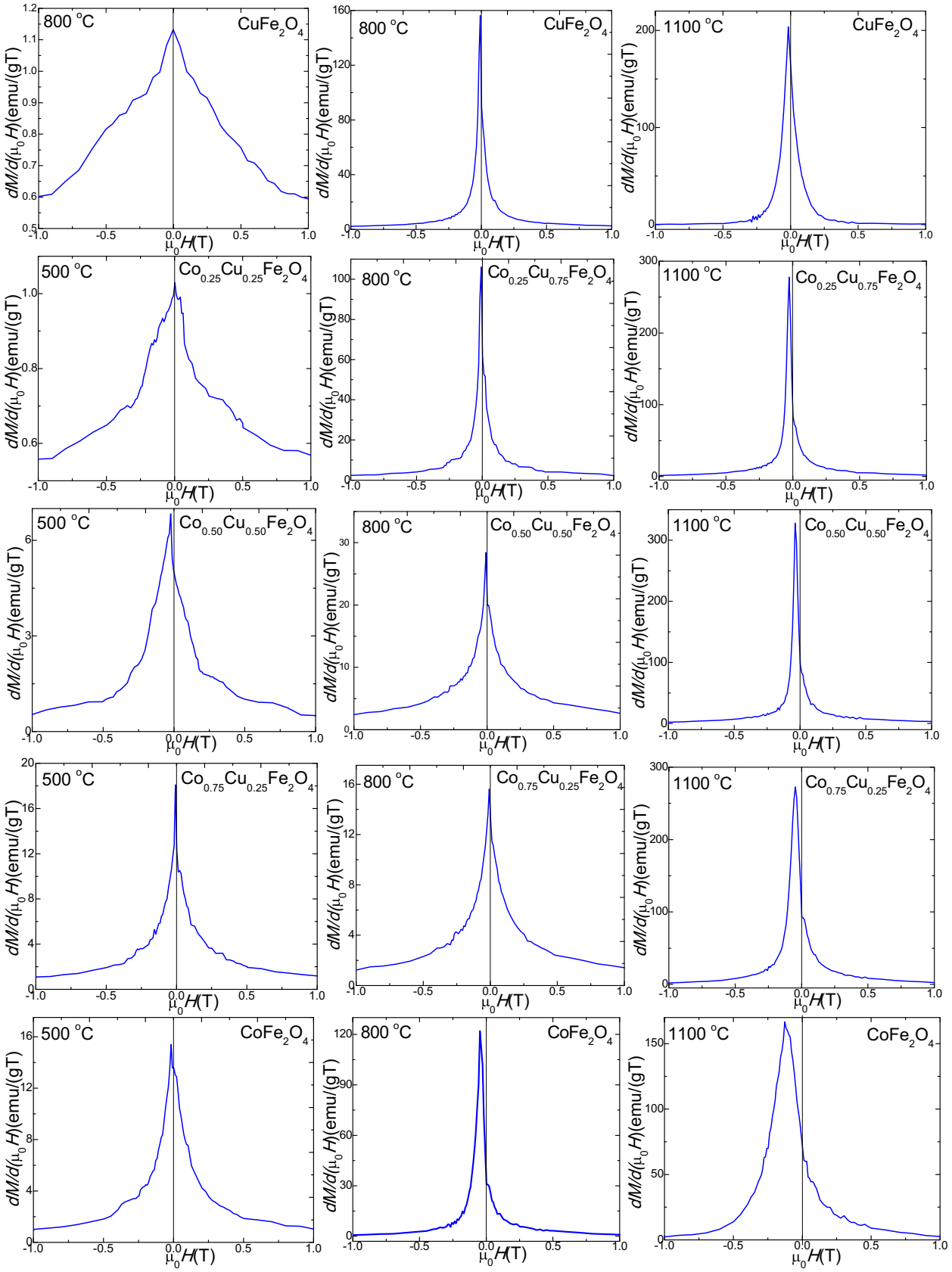

Fig. 7. Magnetization derivatives of $CuFe_2O_4/SiO_2$, $Co_{0.25}Cu_{0.75}Fe_2O_4/SiO_2$, $Co_{0.50}Cu_{0.50}Fe_2O_4/SiO_2$, $Co_{0.75}Cu_{0.25}Fe_2O_4/SiO_2$, $CoFe_2O_4/SiO_2$ NCs annealed at 500, 800 and 1100 °C.

Acknowledgements

This work was supported by the Romanian Ministry of Research and Innovation through Institutional Performance-Projects for Financing Excellence in RDI (grant number 19PFE/2018), Complex Frontier Research Projects (grant number 6/2018 PN-III-P4-ID-PCCF-2016-0112) and Researcher Mobility (grant number 117MC/2019). The authors would like to express their gratitude to Dr. Razvan Hirian and Marc du Plessis for the magnetic measurements and Dr. Lucian Barbu-Tudoran for the SEM and TEM measurements.

References

[1] J. Balavijayalakshmi, N. Suriyanarayanan, R. Jayapraksah, Influence of copper on the magnetic properties of cobalt ferrite nano particles, Mater. Lett. 81 (2012) 52–54, https://doi.org/10.1016/j.matlet.2012.04.076.

[2] M.A. Dar, D. Varshney, Effect of d-block element Co^{2+} substitution on structural, Mössbauer and dielectric properties of spinel copper ferrites, J. Magn. Magn. Mater. 436 (2017) 101–112, https://doi.org/10.1016/j.jmmm.2017.04.046.

[3] B. Chandra Sekhar, G.S.N. Rao, O.F. Caltun, B. Dhana Lakshmi, B. Parvatheeswara Rao, P.S.V. Subba Rao, Magnetic and magnetostrictive properties of Cu substituted Co-ferrites, J. Magn. Magn. Mater. 339 (2016) 59–63, https://doi.org/10.1016/j.jmmm.2015.09.028.

[4] A. Manikandan, R. Sridhar, S. Arul Antony, S. Ramakrishna, A simple aloe vera plant-extracted microwave and conventional combustion synthesis: morphological, optical, magnetic and catalytic properties of $CoFe_2O4$ nanostructures, J, Molec. Struct. 1076 (2014) 188–200, https://doi.org/10.1016/j.molstruc.2014.07.054.

[5] A. Manikandan, M. Durka, K. Seevakan, S. Arul Antony, A novel one-pot combustion synthesis and opto-magnetic properties of magnetically separable spinel $Mn_xMg_{1-x}Fe_2O_4$ ($0.0 \leq x \leq 0.5$) nanophotocatalysts, J. Supercond. Nov. Magn. 28 (2015) 1405–1416, https://doi.org/10.1007/s10948-014-2864-x.

[6] A. Manikandan, M. Durka, S. Arul Antony, A novel synthesis, structural, morphological and opto-magnetic characterizations of magnetically separable spinel $Co_xMn_{1-x}Fe_2O_4$ ($0 \leq x \leq 1$) nano-catalyst, J. Supercond. Nov. Magn. 27 (2014) 2841–2857, https://doi.org/10.1007/s10948-014-2771-1.

[7] D. Ghanbari, M. Salavati-Niasari, M. Ghasemi-Kooch, A sonochemical method for synthesis of Fe_3O_4 nanoparticles and thermal stable PVA-based magnetic nanocomposite, J. Ind. Eng. Chem. 20 (2014) 3970–3974, https://doi.org/10.1016/j.jiec.2013.12.098.

[8] A. Sobhani, M. Salavati-Niasari, Synthesis and characterization of $FeSe_2$ nanoparticles and $FeSe_2$/FeO(OH) nanocomposites by hydrothermal method, J. Alloys Compd. 625 (2015) 26–33, https://doi.org/10.1016/j.jalcom.2014.1.079.

[9] D. Ghanbari, M. Salavati-Niasar, Synthesis of urchin-like CdS-Fe_3O_4 nanocomposites and its application in flame retardancy of magnetic cellulose acetate, J. Ind. Eng. Chem. 24 (2015) 284–292, https://doi.org/10.1016/j.jiec.2014.09.043.

[10] S. Ahmadian-Fard-Fini, D. Ghanbari, M. Salavati-Niasari, Photoluminescence carbon dot as a sensor for detecting of *Pseudomonas aeruginosa* bacteria: hydrothermal synthesis of magnetic hollow $NiFe_2O_4$-carbon dots nanocomposite material, J. Compos. B 161 (2019) 564–577, https://doi.org/10.1016/j.compositesb.2018.12.131.

[11] S. Ahmadian-Fard-Fini, D. Ghanbari, O. Amiri, M. Salavati-Niasari, Electro-spinning of cellulose acetate nanofibers/Fe/carbon dot as photoluminescence sensor for mercury (II) and lead (II) ions, Carbohydr. Polym. 229 (2020) 115428, https://doi.org/10.1016/j.carbpol.2019.115428.

[12] M. Salavati-Niasari, J. Hasanalian, H. Najafian, Alumina-supported $FeCl_3$, $MnCl_2$, $CoCl_2$, $NiCl_2$, $CuCl_2$ and $ZnCl_2$ as catalysts for the benzylation of benzene by benzyl chloride, J. Mol. Catal. A Chem. 209 (2004) 209–214, https://doi.org/10.1016/j.molcata.2003.08.027.

[13] A. Abbasi, D. Ghanbari, M. Salavati-Niasari, M. Hamadanian, Photo-degradation of methylene blue: photocatalyst and magnetic investigation of Fe_2O_3-TiO_2 nanoparticles and nanocomposites, J. Mater. Sci-Mater El. 27 (2016) 4800–4809, https://doi.org/10.1007/s10854-016-4361-4.

[14] H.M.K. Tedjieukeng, P.K. Tsobnang, R.L. Fomekong, E.P. Etape, P.A. Joy, A. Delcorte, J.N. Lambia, Structural characterization and magnetic properties of undoped and copper-doped cobalt ferrite nanoparticles prepared by the octanoate coprecipitation route at very low dopant concentrations, RSC Adv. 8 (8) (2018) 38621–38630, https://doi.org/10.1039/C8RA08532C.

[15] K.A. Sampath, T. Himanshu, B. Kevin, S.P. Singh, Structural, magnetic and in vitro bioactivity of Co-Cu ferrite and bioglass composite for hyperthermia in bone tissue engineering, Bioceram. Dev. Appl. 6 (1) (2016) 1–7, https://doi.org/10.4172/2090-5025.100091.

[16] A. Manikandan, M. Durka, M. Amutha Selvi, S. Arul Antony, *Sesamum indicum* plant extracted microwave combustion synthesis and opto-magnetic properties of spinel $Mn_xCo_{1-x}Al_2O_4$ nano-catalyst, J. Nanosci. Nanotechnol. 16 (2016) 448–456, https://doi.org/10.1166/jnn.2016.10632.

[17] M.A. Almessiere, Y. Slimani, H. Güngüneş, A. Manikandan, I. Ercan, A. Baykal, A.V. Trukhanov, Magnetic attributes of $NiFe_2O_4$ nanoparticles: influence of dysprosium ions (Dy^{3+}) substitution, Nanomaterials 9 (6) (2019) 820, https://doi.org/10.3390/nano9060820.

[18] S.M. Ansari, S.R. Suryawanshi, M.A. More, D. Sen, Y.D. Kolekar, C.V. Ramana, Field emission properties of nano-structured cobalt ferrite ($CoFe_2O_4$) synthesized by low-temperature chemical method, Chem. Phys. Lett. 701 (2018) 151–156, https://doi.org/10.1016/j.cplett.2018.04.027.

[19] M.P. Ghosh, S. Mukherjee, Microstructural, magnetic, and hyperfine characterizations of Cu-doped cobalt ferrite nanoparticles, J. Am. Chem. Soc. 102 (2019) 7509–7520, https://doi.org/10.1111/jace.16687.

[20] M. Stefanescu, T. Dippong, M. Stoia, O. Stefanescu, Study on the obtaining of cobalt oxides by thermal decomposition of some complex combination, undispersed and dispersed in SiO_2 matrix, J. Therm. Anal. Cal. 94 (2) (2008) 389–393, https://doi.org/10.1007/s10973-008-9111-2.

[21] T. Dippong, F. Goga, E.A. Levei, O. Cadar, Influence of zinc substitution with cobalt on thermal behavior, structure and morphology of zinc ferrite embedded in silica matrix, J. Solid State Chem. 275 (2019) 159–166, https://doi.org/10.1016/j.jssc.2019.04.011.

[22] G.J. Owens, R.K. Singh, F. Foroutan, M. Alqaysi, C.M. Han, C. Mahapatra, H.W. Kim, J.C. Knowles, Sol–gel based materials for biomedical applications, Prog. Mater. Sci. 77 (2016) 1–79, https://doi.org/10.1016/j.pmatsci.2015.12.001.

[23] M. Amir, H. Gungunes, A. Baykal, M.A. Almessiere, H. Sözeri, I. Ecran, M. Sertkol, S. Asiri, A. Manikandan, Effect of annealing temperature on magnetic and Mössbauer properties of $ZnFe_2O_4$ nanoparticles by sol-gel approach, J. Supercond. Nov. Magn. 31 (2018) 3347–3356, https://doi.org/10.1007/s10948-018-4610-2.

[24] P. Bhavani, A. Manikandan, P. Paulraj, A. Dinesh, A. Durka, S. Arul Antony, Okra (*Abelmoschus esculentus*) plant extract-assisted combustion synthesis and characterization studies of spinel $ZnAl_2O_4$ nano-catalysts, J. Nanosci. Nanotechno. 18 (2018) 4072–4081, https://doi.org/10.1166/jnn.2018.15217.

[25] M. Hashim, Alimuddin, S. Kumar, B.H. Koo, S.E. Shirsath, E.M. Mohammed, J. Shah, R.K. Kotnala, H.K. Choi, H. Chun, R. Kumar, Structural, electrical and magnetic properties of Co-Cu ferrite nanoparticles, J. Alloys Compd. 518 (2012) 11–18, https://doi.org/10.1016/j.jallcom.2011.12.017.

[26] T. Dippong, I.G. Deac, O. Cadar, E.A. Levei, L. Diamandescu, G. Borodi, Effect of Zn content on structural, morphological and magnetic behavior of $Zn_xCo_{1-x}Fe_2O_4/SiO_2$ nanocomposites, J. Alloy. Compd. 792 (2019) 432–443, https://doi.org/10.1016/j.jallcom.2019.04.059.

[27] Joint Committee on Powder Diffraction Standards-International Center for Diffraction Data, (1999).

[28] M. Margabandhu, S. Sendhilnathan, S. Senthilkumar, D. Gajalakshmi, Investigation of structural, morphological, magnetic properties and biomedical applications of Cu^{2+} substituted uncoated cobalt ferrite nanoparticles, Braz. Arch. Biol. Technol. 59 (2) (2016) 1–10, https://doi.org/10.1590/1678-4324-2016161046.

[29] A.A. Bagade, V.V. Ganbavle, S.V. Mohite, T.D. Dongale, B.B. Sinha, K.Y. Rajpure, Assessment of structural, morphological, magnetic and gas sensing properties of $CoFe_2O_4$ thin films, J. Colloid Interface Sci. 497 (2017) 181–192, https://doi.org/10.1016/j.jcis.2017.02.067.

[30] A. Jagminas, K. Mažeika, R. Kondrotas, M. Kurtinaitienė, A. Jagminienė, A. Mikalauskaitė, Functionalization of cobalt ferrite nanoparticles by a vitamin C-assisted covering with gold, Nanomater. Nanotechnol. 4 (1) (2014) 1–9, https://doi.org/10.5772/58453.

[31] T. Dippong, E.A. Levei, C. Tanaselia, M. Gabor, M. Nasui, L. Barbu Tudoran, G. Borodi, Magnetic properties evolution of the $Co_xFe_{3-x}O_4/SiO_2$ system due to advanced thermal treatment at 700 °C and 1000 °C, J. Magn. Magn. Mater. 410 (2016) 47–54, https://doi.org/10.1016/j.jmmm.2016.03.020.

[32] B.D. Cullity, C.D. Graham, Introduction to Magnetic Materials, John Wiley & Sons, Inc, Hoboken, New Jersey, 2019, p. 359.

[33] T. Dippong, O. Cadar, I.G. Deac, M. Lazar, G. Borodi, E.A. Levei, Influence of ferrite to silica ratio and thermal treatment on porosity, surface, microstructure and magnetic properties of $Zn_{0.5}Ni_{0.5}Fe_2O_4/SiO_2$ nanocomposites, J. Alloys Compd. 828 (2020) 154409, , https://doi.org/10.1016/j.jallcom.2020.154409.